Structure of ^{14}C and ^{14}B from the ^{14,15}C$(d,^3$He$)^{13,14}$B reactions

S. Bedoor,[1,2,*] A. H. Wuosmaa,[1,2,†] M. Albers,[3] M. Alcorta,[3,‡] Sergio Almaraz-Calderon,[3,§] B. B. Back,[3] P. F. Bertone,[3,‖] C. M. Deibel,[4] C. R. Hoffman,[3] J. C. Lighthall,[1,‡] S. T. Marley,[1,3,¶] D. G. Mcneel,[2] R. C. Pardo,[3] K. E. Rehm,[3] J. P. Schiffer,[3] and D. V. Shetty[5]

[1]*Department of Physics, Western Michigan University, Kalamazoo, Michigan 49008-5252, USA*
[2]*Department of Physics, University of Connecticut, Storrs, Connecticut 06268-3046, USA*
[3]*Physics Division, Argonne National Laboratory, Argonne, Illinois 60439, USA*
[4]*Department of Physics and Astronomy, Louisiana State University, Baton Rouge, Louisiana 70803, USA*
[5]*Department of Physics, Grand Valley State University, Allendale, Michigan 49401, USA*

(Received 4 March 2016; published 21 April 2016)

We have studied the ^{14,15}C$(d,^3$He$)^{13,14}$B proton-removing reactions in inverse kinematics. The $(d,^3$He) reaction probes the proton occupation of the target ground state, and also provides spectroscopic information about the final states in ^{13,14}B. The experiments were performed using ^{14,15}C beams from the ATLAS accelerator at Argonne National Laboratory. The reaction products were analyzed with the HELIOS device. Angular distributions were obtained for transitions from both reactions. The ^{14}C-beam data reveal transitions to excited states in ^{13}B that suggest configurations with protons outside the $\pi(0p_{3/2})$ orbital, and some possibility of proton cross-shell $0p$-$1s0d$ excitations, in the ^{14}C ground state. The ^{15}C-beam data confirm the existence of a broad 2^- excited state in ^{14}B. The experimental data are compared to the results of shell-model calculations.

DOI: 10.1103/PhysRevC.93.044323

I. INTRODUCTION

The questions of the filling of states in light nuclei, and in particular whether six nucleons in ^{12}C complete the $p_{3/2}$ subshell, have existed since the early days of the shell model and the discussion of intermediate coupling [1]. Spectroscopic factors from studies of neutron-removal reactions, for example, (p,d) [2], $(^3$He,$\alpha)$ [3], and (d,t) [4,5], suggest that the occupation of the $p_{1/2}$ neutron subshell is at least 20% as much as the $p_{3/2}$. The data for proton removal with the $(d,^3$He) reaction are consistent with this observation for ^{12}C [6]. Away from $A = 12$, however, the proton $p_{1/2}$ occupancy seems to change significantly, to approximately 3% of the ground-state value for ^{14}C [6]. In the mirror nucleus ^{14}O, the corresponding neutron $p_{3/2}$ occupancy measured with the ^{14}O$(d,t)^{13}$O reaction agreed with theoretical expectations [7] when a renormalization consistent with that obtained from other analyses (see [8,9]) was applied, although no direct measurement of the neutron $p_{1/2}$ occupancy was reported. This change to a more nearly closed $p_{3/2}$ subshell for $A = 14$ was already suggested from early calculations of spectroscopic factors for transfer reactions in the $0p$ shell [10].

The ^{14}C measurements reported in [6] suffered, however, from a 60% ^{12}C impurity in the ^{14}C target; reactions on the ^{12}C made identification of weak transitions to excited states in ^{13}B difficult or impossible. In that work no evidence of proton cross-shell configurations was found in the ground states of any of the carbon isotopes studied. This result was perhaps not surprising because of the large expected $0p_{3/2} - sd$ energy gap for protons. It was known for some time [11] that in light nuclei the neutron shell gaps change dramatically with Z including a reordering of the $1s_{1/2}$ and $0d_{5/2}$ orbitals between ^{17}O and ^{15}C. The experimental results on this behavior were recently summarized [12].

The detailed level structure of ^{13}B is not particularly well known, although recent studies of ^{13}B with unstable beams have provided additional information about the spins and parities of some excited states. The ^{12}B$(d,p)^{13}$B reaction [13] was used to determine the spins of the two lowest positive-parity neutron excitations first observed in the ^{11}B$(t,p)^{13}$B reaction at 3.48 and 3.68 MeV. A recent lifetime measurement has suggested that the lowest negative-parity excited state at 3.53 MeV had $J^\pi = 3/2^-$ and possessed neutron $2p-2h$ character [14]. Finally, a $J^\pi = 1/2^+$ proton-"intruder" state was reported in ^{13}B from the ^{14}Be$(\alpha,t)^{13}$B reaction [15] at 4.83-MeV excitation energy. Population of this state in the ^{14}C$(d,^3$He$)^{13}$B reaction may suggest some admixtures of proton-$(sd)^2$ configurations in the ^{14}C ground state.

One goal of the present work is to search for transitions in the ^{14}C$(d,^3$He$)^{13}$B reaction that could not be observed in the experiment described in Ref. [6]. We performed this measurement in inverse kinematics so no interfering transitions from impurities exist.

Considerably less is known about ^{14}B. ^{14}B is the lightest particle-bound $N = 9$ isotone. The low-lying levels are $(1s_{1/2}0d_{5/2})$ valence-neutron states; coupling to a proton-$0p_{3/2}$ hole produces two 2^-, two 1^-, one 3^-, and one 4^- state, and the pairs of 2^- and 1^- states are configuration mixed. Previous studies of the ^{13}B$(d,p)^{14}$B reaction determined the

*Present address: Texas A&M University, College Station, TX 77843-4242, USA.
†Corresponding author: alan.wuosmaa@uconn.edu
‡Present address: TRIUMF, Vancouver, BC V6T 2A3, Canada.
§Present address: Florida State University, Tallahassee, FL 32306 USA.
‖Present address: Marshall Space Flight Center, Huntsville, AL 35811, USA.
¶Present address: Louisiana State University, Baton Rouge, LA 70803-4001, USA.

$\ell = 0$ and 2 neutron strengths for the ground 2^-_1, and excited 1^-_1, 3^-_1, and 4^-_1 states [16]. The 2^-_1 and 1^-_1 levels were predominantly $\ell = 0$. The expected $2^-_2/1^-_2$ pair, dominated by $\nu(0d_{5/2})$ configurations, was not observed in the (d,p) measurements, although a broad ($\Gamma \approx 1$ MeV) 2^-_2 state does appear in the literature near 2 MeV from various reactions [17]. That broad state would have been obscured by much stronger transitions to the 3^-_1 and 4^-_1 levels in (d,p). No information exists about a possible second 1^- state. While the 2^-_2 and 1^-_2 levels were not observed in the (d,p) measurement, their $1s_{1/2}$ and $0d_{5/2}$ neutron spectroscopic factors could still be estimated in a two-state mixing model.

Other aims of this work are to confirm the reported 2^-_2 state, and to compare the proton-removal strength for different ^{14}B excitations to expectations based on the earlier (d,p) measurements. Because of the $1s_{1/2}$ single-particle character of the ^{15}C ground state, the strongest transitions in ^{15}C$(d,^3$He$)^{14}$B will be to final states with large $1s_{1/2}$ neutron strength. The 3^-_1 and 4^-_1 levels that obscured the excited 2^- state in the (d,p) study are neutron $\ell = 2$ excitations that should be absent in $(d,^3$He$)$. Because the present ^{15}C beam intensity is low, weaker transitions to states with proton configurations other than $\pi(0p_{3/2})^{-1}$ will be difficult to observe.

In this paper we first present experimental details, followed by a description of the data reduction process including Monte Carlo simulations of the response of the apparatus. We then give a distorted wave Born approximation (DWBA) reaction-model analysis of the angular distributions to extract spectroscopic factors. Finally, we discuss our results in the context of shell-model calculations.

II. EXPERIMENT

The ^{14,15}C$(d,^3$He$)^{13,14}$B reactions were studied in inverse kinematics at the ATLAS facility at Argonne National Laboratory. The reaction products were analyzed using the helical orbit spectrometer (HELIOS) [18,19]. HELIOS is a solenoidal spectrometer designed to study transfer and other reactions in inverse kinematics.

A. Secondary-beam production

The ^{14}C ($T_{1/2} = 5{,}730 \pm 40$ year) beam was produced from enriched ^{14}C material in a Cs sputter source. The ^{14}C energy was 17.1 AMeV, and for the ^{14}C$(d,^3$He$)^{13}$B experiment the beam intensity was approximately 0.1 pnA. The ^{15}C beam was made using the in-flight method described in Refs. [20,21]. To produce the secondary beam, the ^{14}C primary-beam intensity was increased to 100 pnA. This beam bombarded a cryogenic D_2 gas cell held at a pressure of 1400 mbar and at a temperature of $-184\,^\circ$C. The ^{15}C beam was made from $d(^{14}$C$,^{15}$C$)p$ ($Q = -1.007$ MeV) reactions in the cell. The resulting ^{15}C beam of approximately 5×10^5 particles/s had an energy of 15.7 AMeV. The high bombarding energies, which were the greatest available from the accelerator at the time, were chosen because of the very negative Q values of -15.337 and -15.586 MeV of the ^{14}C$(d,^3$He$)^{13}$B and ^{15}C$(d,^3$He$)^{14}$B reactions. The secondary-beam contained small impurities from lower charge states of the primary ^{14}C ions ($\approx 3\%$), and from isotopes of Be ($\approx 1\%$). Events from these impurity beams were eliminated by requiring coincidences between ^{3}He ions and identified ^{13,14}B reaction products as described below.

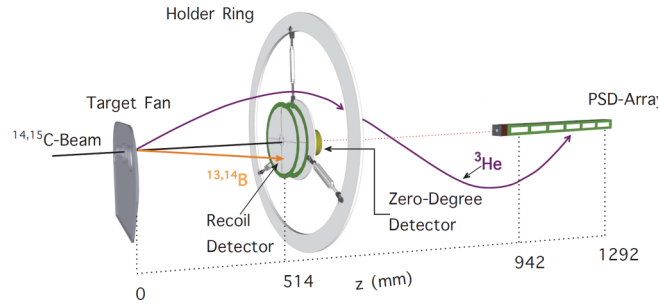

FIG. 1. Schematic diagram of the experimental setup.

B. Experimental setup

The experimental setup was identical to that described in [22]. A schematic diagram of the experimental setup appears in Fig. 1. HELIOS consists of a superconducting solenoid with a bore diameter of 920 mm and length of 2350 mm that produces an approximately uniform magnetic field aligned with the beam direction. For this measurement, the field strength was 2.5 T. The ^{14,15}C beams bombarded solid deuterated-polyethylene $[(CD_2)_n]$ foil targets of areal density 140 μg/cm^2 placed on the magnetic axis near the entrance of the solenoid, 550 mm upstream of the geometric center of the magnet ($z_{tgt} = -550$ mm). The ^{3}He particles emerged in the forward hemisphere with laboratory angles less than 35°. These particles were transported in helical trajectories to an array of 24 position-sensitive silicon detectors (PSDs) that surrounded the beam in the downstream end of the magnet. The PSD array subtended distances between 940 and 1290 mm from the target. These detectors registered the energies of the ^{3}He ions, the distances from the target at which they returned to the solenoid axis, and the particle flight times. The ^{3}He time of flight was approximately equal to the cyclotron period $T_{\rm CYC} = 39.3$ ns. Deviations of the flight time from $T_{\rm CYC}$ arose for very small-angle trajectories that intercepted the PSD array a significant distance from where they would return to the solenoid axis. Other distortions in the helical orbits arose from particles traveling through nonuniform regions of the magnetic field, however, the geometry for this measurement confined the ^{3}He ions to volumes where the field differed from the maximum value by at most 5%.

Additional information about the reaction was provided by a set of silicon-detector ΔE-E telescopes positioned between the target and the PSD array. These detectors were perpendicular to the beam direction, and detected and identified the ^{14,13,12,11}B reaction products. The telescopes covered the full 2π azimuthal angle except for four 8°-wide gaps from their mounting structure, and subtended laboratory polar angles between 1° and 5°. The thicknesses of the ΔE and E layers were 500 μm and 1000 μm, respectively.

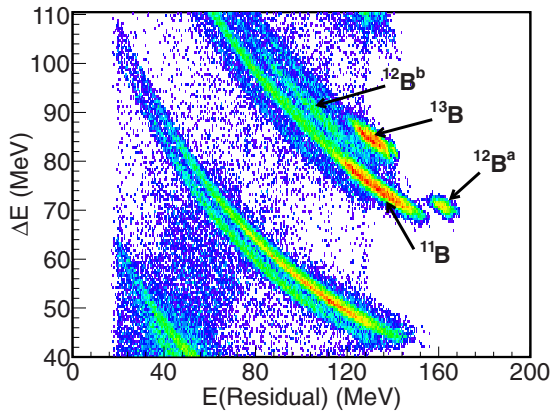

FIG. 2. Silicon-detector telescope particle-identification spectrum obtained with the ^{14}C beam incident on the $(CD_2)_n$ target. The heavy particles are in coincidence with a particle in the HELIOS PSD array. The groups labeled ^{13}B and ^{12}B^{b} are from particle-bound and unbound states in ^{13}B; the groups labeled ^{12}B^{a} and ^{11}B are from particle-bound and unbound states in ^{12}B from the (d,α) reaction.

A representative particle-identification spectrum from these detectors for $^{14}C+CD_2$ collisions appears in Fig. 2. Here, the events include a light particle detected in the HELIOS PSD array. The resolution was sufficient to identify all of the boron isotopes of interest and the different reaction channels. Because of this good resolution, the time-of-flight information for the light-charged particles in the PSD array was not used in the analysis. In Fig. 2, ^{12}B ions from both the (d,α) reaction (labeled ^{12}B^{a}) and from neutron-unbound states in ^{13}B from the $(d,^3\mathrm{He})$ reaction (labeled ^{12}B^{b}) are present. The strong ^{11}B group arises from neutron-unbound states in ^{12}B from the ^{14}C$(d,\alpha)^{12}$B reaction. Results for the ^{14,15}C$(d,\alpha)^{12,13}$B reactions have been presented elsewhere [22].

The incident beam flux was monitored by using a silicon surface-barrier (SSB) detector mounted on the recoil-detector assembly at 0°. A tantalum sheet 0.5-mm thick, with regularly spaced 80-μm diameter holes at intervals of 2.5 mm, was used in front of the SSB telescope to attenuate the beam flux by a factor of approximately 1000 to keep the monitor count rate at a manageable level. For the stable-beam experiments, the beam spot was less than 2 mm in diameter, a size comparable to the hole spacing. The count rate in that detector was thus extremely sensitive to the beam-spot size and position and the deduced value of the integrated beam flux was not usable for normalization purposes. The secondary-beam spot was larger, approximately 5 mm in diameter, and so for the secondary beam the ion-flux measurements were reliable at the 30% to 50% level. A procedure for determining the absolute yields for the ^{14}C measurements is described below.

Information for any event with a particle detected in the HELIOS PSD array was recorded for all detectors. Subsets of events where only a heavy recoil was detected in the ΔE-E telescope or a beam particle triggered the 0° monitor detector were also recorded. Calibration information for the PSD array was provided by a mixed ^{148}Gd-^{244}Cm source, as well as by data for known transitions from the ^{14}C$(d,^{3,4}\mathrm{He})^{13,12}$B reactions.

III. DATA REDUCTION AND ANALYSIS

In HELIOS, for a given excitation energy the laboratory kinetic energy of the detected particle depends linearly on the distance between the target and the point at which the particle is detected near the solenoid axis ("z"). The kinematic loci for different excited states appear as diagonal lines in the $E(^3\mathrm{He})$ vs z plane. Figure 3 shows spectra of energy-versus-position for the ^{14}C$(d,^3\mathrm{He})^{13}$B reaction for events where the ^{3}He was in coincidence with an identified ^{13}B(a) or ^{12}B(b) ion. The vertical gaps correspond to spaces between the PSDs.

For comparison, Fig. 4 shows a Monte Carlo simulation of the response of the apparatus for several transitions in the ^{14}C$(d,^3\mathrm{He})^{13}$B reaction. Equal numbers of events for each transition were used in the simulations. Figures 4(a) and 4(b) have the same significance as in Fig. 3. The simulation includes the detector geometry and energy-loss effects in the target, and tracks both the ^{3}He and recoil particles through a magnetic field described in Ref. [19]. The excitation energies used in the calculation are from the analysis outlined below. The line for the ground state is straight. For the excited states, however, the ^{3}He particles have shallower orbits and intercept

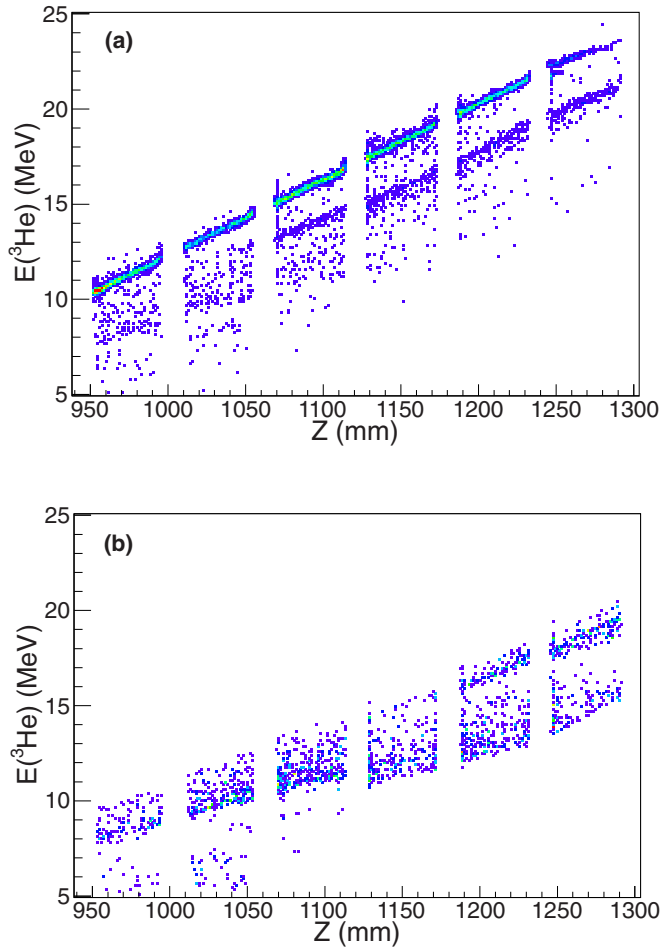

FIG. 3. Energy-versus-position spectra for ^{3}He particles from the ^{14}C$(d,^3\mathrm{He})^{13}$B reaction. (a) Data for ^{3}He$+^{13}$B coincidence events. (b) Data for ^{3}He$+^{12}$B coincidence events. Further analysis on the unbound states includes only data taken for $z > 1180$ mm.

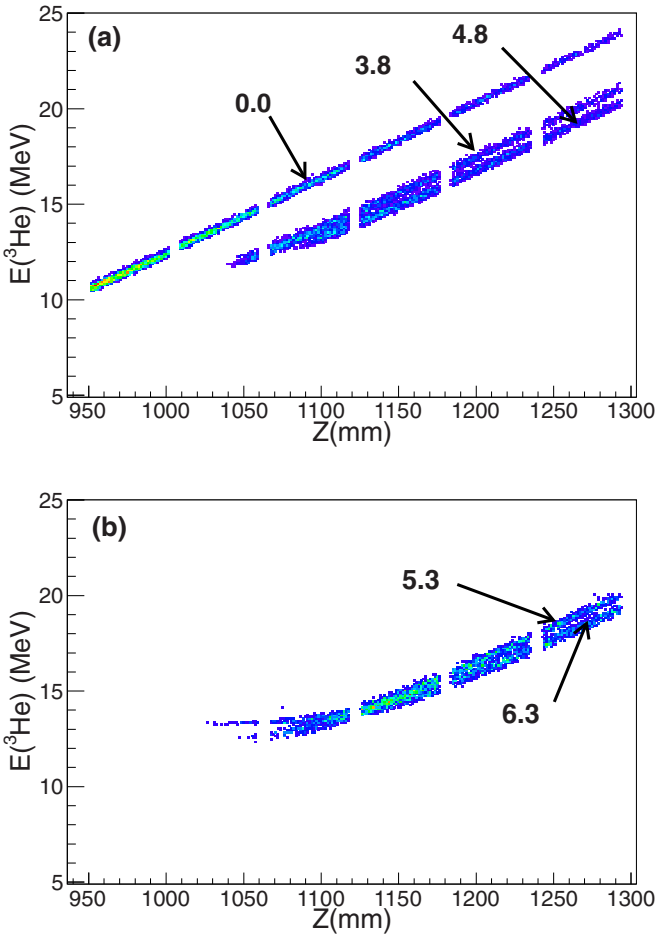

FIG. 4. Monte Carlo simulations of energy-versus-position spectra for ^{3}He particles from the ^{14}C$(d,^{3}$He$)^{13}$B reaction. (a) Simulated data for ^{3}He$+^{13}$B coincidence events. (b) Simulated data for ^{3}He$+^{12}$B coincidence events. The excitation energies used in the calculations are indicated on the figure.

the silicon array at shorter distances from the target than in the ideal situation, causing the loci for different states to merge between $z \approx 1050$ mm and 1180 mm, depending on the excitation energy. The cutoff of the lines for the excited states near $z = 1050$ mm arises from the recoil-coincidence acceptance where the corresponding boron ions go through the central hole in the ΔE-E telescope and are not detected.

Figure 5 shows similar results from the ^{15}C$(d,^{3}$He$)^{14}$B reaction. Events for the ^{15}C-induced reactions are shown using different symbols depending on whether the coincident recoil ion was ^{14}B (black circles, residual nucleus bound), or ^{13}B (red squares, residual nucleus unbound). The experimental geometry was optimized for the ^{15}C-beam measurement. For that reaction the ^{3}He particles cover the entire PSD array without deviations of the kinematic loci from linear behavior.

A. Excitation-energy spectra

Excitation-energy spectra for the ^{14,15}C$(d,^{3}$He$)^{13,14}$B reactions, obtained from projections of the data shown in Figs. 3 and 5 appear in Figs. 6 and 7. For Fig. 6, the data are taken only

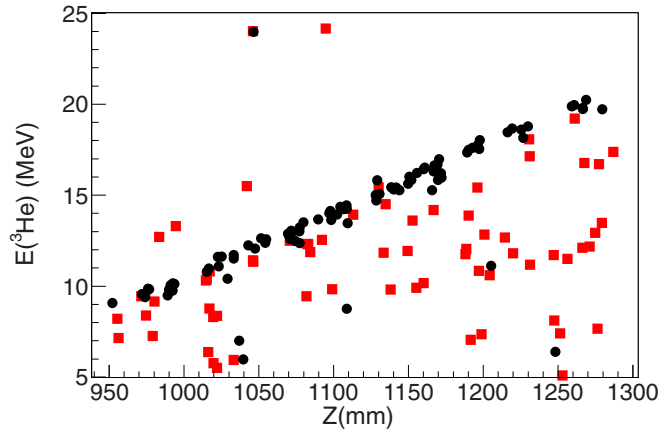

FIG. 5. Energy-versus-position spectra for ^{3}He particles from the ^{15}C$(d,^{3}$He$)^{14}$B reaction. The black circles and red squares correspond to ^{3}He $+^{14}$B and ^{3}He $+^{13}$B coincidence events, respectively.

from detectors where the Monte Carlo simulations indicate that all trajectories are parallel. Only data for positions where the transitions can be resolved in excitation energy are used in the subsequent analysis. Figures 6(a) and 6(b), and 7(a) and 7(b) represent data obtained for (a) particle-bound, and (b) particle-unbound states. The neutron-separation energies are $S_n = 4.878$ MeV and 0.969 MeV for ^{13}B and ^{14}B, respectively. The excitation-energy resolution for the ^{14}C spectrum is

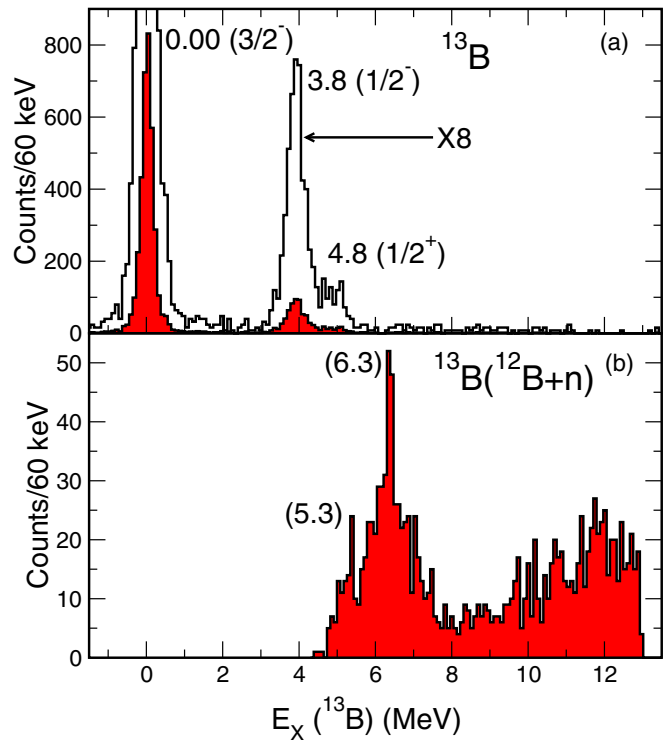

FIG. 6. ^{13}B excitation-energy spectra from the ^{14}C$(d,^{3}$He$)^{13}$B reaction. (a) Events in coincidence with identified ^{13}B ions with the open histogram displaying the same data multiplied by a factor of 8 to enhance weak transitions. (b) Events in coincidence with identified ^{12}B ions.

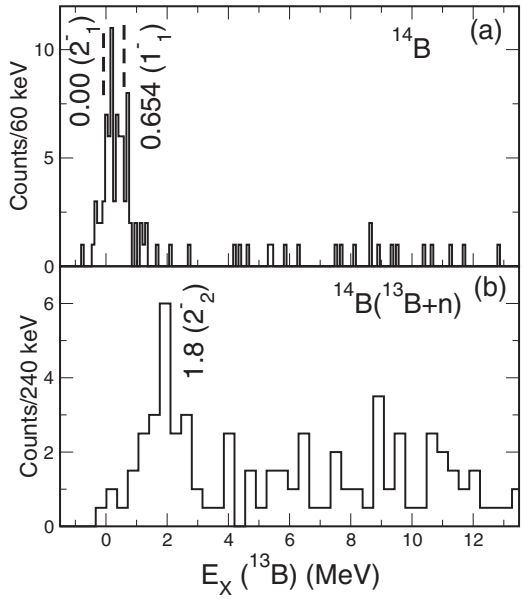

FIG. 7. ^{14}B excitation-energy spectra from the ^{15}C$(d,^3$He$)^{14}$B reaction. (a) and (b) Particle-bound (unbound) states obtained in coincidence with identified ^{14}B (^{13}B) ions.

approximately 180-keV full width at half maximum (FWHM), dominated by detector resolution, kinematic shift, and energy loss in the target. For the ^{15}C data, the estimated excitation-energy resolution includes an additional 140-keV contribution from the spread in the energy of the secondary beam caused by energy loss and straggling in the production cell, resulting in a value of 240-keV FWHM when the contributions are added in quadrature.

1. $^{14}C \rightarrow {}^{13}B$

In Fig. 6(a) the filled and open histograms represent the same data; the open histogram was multiplied by a factor of 8 to illustrate the weaker transitions. For comparison, Table I lists states reported in the literature for ^{13}B and ^{14}B. The strongest transition in the ^{14}C$(d,^3$He$)^{13}$B reaction is to the ^{13}B ground state. The next strongest transition at $E_X = 3.8$ MeV likely corresponds to the presumed $1/2^-$ state at 3.71 MeV reported in Ref. [6]. The suggested neutron-intruder $(3/2^-)$ (3.53 MeV) state would have a $\nu(1s_{1/2})^2$ configuration, and the positive-parity states at 3.48 and 3.68 MeV are dominantly $\nu(1s0d)$-neutron excitations; none of these should be strongly populated in this reaction.

We cannot rule out some contribution to the 3.8-MeV peak from the state reported at $E_X = 4.13$ MeV which has no assigned spin or parity, and would not be well resolved from the $1/2^-$ in our measurement. A small peak also appears near $E_X = 4.8$ MeV, which must be below the neutron-separation energy of 4.878 MeV as it appears in coincidence with identified ^{13}B ions. This state likely corresponds to the possible $1/2^+$ state reported at 4.83 MeV. We observe two peaks in the spectrum of neutron-unbound states, one very weak transition at $E_X \approx 5.3$ MeV and another slightly stronger one at $E_X \approx 6.3$ MeV. For comparison, states are reported in the literature

TABLE I. Excitation energies, spins, and parities of states in ^{13}B and ^{14}B from the present measurement and from the literature (from [23] unless otherwise noted).

^{13}B				
	Data		Literature	
State	E_X (MeV)	J^π	E_X (MeV)	J^π
0	0.0	$3/2^-$	0.00	$3/2^-$
			3.48	$(1/2^+)$[a]
			3.53	$(3/2^-)$[b]
			3.68	$(3/2,5/2)^+$[a]
1	3.8	$(1/2^-)$	3.71	$1/2^-$[c]
			4.13	
2	4.8	$(1/2^+)$	4.83	$(1/2^+)$[d]
			$S_n = 4.878$ MeV	
			5.02	
3	5.3	$(1/2,3/2)^-$	5.11	
			5.39	
			5.56	
			6.17	
4	6.3	$\pi = +$	6.43	
			6.93	
^{14}B				
	0.000	2^-	0.000	2^-
	0.654[e]	1^-	0.654[e]	1^-
			$S_n = 0.969$ MeV	
			1.380	3^-
	1.80	(2^-)	1.860	2^-
			2.080	4^-
			2.320	
			2.970	

[a]From Ref. [13].
[b]From Ref. [14].
[c]From Ref. [6].
[d]From Ref. [15].
[e]From Ref. [24].

at 5.02, 5.11, 5.39, 6.17, and 6.43 MeV, none of which has a spin-parity assignment. The excitation-energy resolution of the present measurement does not permit a firm identification of the peaks observed here with previously known levels. We also observe strength at higher excitation energies that could represent transitions to even higher excited states, however, given the limited acceptance and poor statistics it is not possible to make any further statements about this yield.

To provide more information about the observed peaks, the boron excitation energies deduced from the ^{3}He energy and position can be correlated with the boron-recoil energies. Figure 8 shows this correlation for data obtained with the ^{14}C beam, and from the Monte Carlo simulations described above. The bound states labeled (0), (1), and (2) correspond to excitation energies of 0.0, 3.8, and 4.8 MeV, respectively. For these excitations the recoil energies are near $E_{\text{recoil}} = 200$ MeV with a narrow spread in E_{recoil}. For unbound states at $E_X = 5.3$ (3) and 6.3 (4) MeV, the recoil energies are smaller and the distributions in E_{recoil} are wider because of the kinetic energy lost to neutron emission. Although the peaks at 4.8 MeV (2) and 5.3 MeV(3) are not fully resolved in excitation energy, the

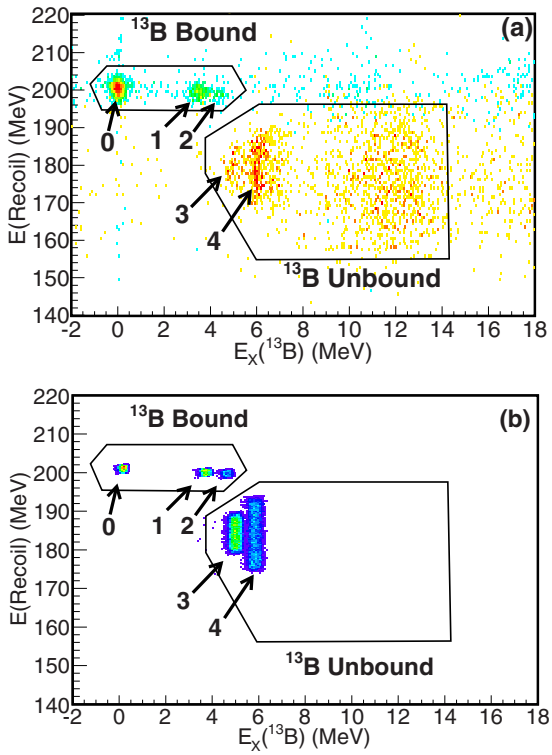

FIG. 8. Correlation between boron recoil energy and reconstructed ^{13}B excitation energy. (a) Data (b) Monte Carlo simulation. The polygons illustrate the regions corresponding to bound and unbound states in ^{13}B and are not used as event-selection criteria in the analysis. The labels (0)–(4) correspond to excitations in ^{13}B listed in Table I.

correlation with the recoil energy permits their separation and shows that they are distinct transitions.

2. $^{15}C \rightarrow {}^{14}B$

For ^{14}B, in Table I we accept the spin-parity assignments as given in the literature. The ground 2^-_1 and first-excited 1^-_1 (0.654 MeV) [24] are not fully resolved in the present measurement. As discussed in the introduction, these two levels are predominantly $\ell = 0$ $1s_{1/2}$ states, and both should be strongly populated in this reaction. Beyond the neutron-decay threshold, the statistics are limited. The most prominent feature is a broad ($\Gamma \approx 1$ MeV) peak at $E_X = 1.8 \pm 0.3$ MeV which presumably corresponds to the 1.86-MeV 2^-_2 state reported in the ^{14}C(^{7}Li,^{7}Be)^{14}B reaction [17]. While this state was not observed in the (d,p) reaction the estimated relative neutron-stripping spectroscopic factors suggested that the $1s_{1/2}$ strength in the 2^-_2 state was roughly 20% of that of the ground state [16]. Shell-model calculations for neutron stripping suggested a slightly higher value, nearer to 30%. Assuming that the ^{15}C ground-state neutron wave function is pure $1s_{1/2}$, a rough estimate suggests that the 2^-_2 state should appear with approximately 20%–30% of the intensity of the ground state. With even less $1s_{1/2}$ strength, the expected 1^-_2 state will be more weakly populated. Shell-model calculations described below also suggest that this level exists between 3- and 4-MeV excitation energy, making it broader and even more difficult to identify in the present data than the 2^-_2 excitation.

IV. RESULTS AND INTERPRETATION

A. Angular distributions

Angular distributions were produced from the measured yields, taking into account the solid angles of the PSDs, which for a given excitation energy are approximately equal for each detector. The recoil-coincidence detection efficiency was determined from the Monte Carlo simulations described above. This efficiency depends on scattering angle and excitation energy, and whether the final state is neutron bound or unbound. Typical values range between 0.60 and 0.90. Small corrections to the calculated center-of-mass angles depending on position and excitation energy, typically ranging from 1 to 2 degrees, were also obtained from Monte Carlo simluations.

The absolute normalizations for the ^{14}C and ^{15}C data were determined in different ways. As discussed above, for the ^{14}C-beam data the measurement of the absolute beam intensity was unreliable. The absolute cross-section scale for the present ^{14}C data was determined by combining the measured ground-state angular distribution from Ref. [6] with an estimate of the dependence of the cross section on bombarding energy from DWBA calculations. The calculations were done using the finite-range code PTOLEMY [25] with optical-model parameters for the entrance and exit channels obtained from global analyses with energy-dependent well depths [26,27]. The form factor for the $d - {}^3$He vertex was obtained from the results of Green's-function Monte Carlo calculations in the manner described in Ref. [28]. Figure 9 shows the $(d,{}^3\mathrm{He})$ data of Ref. [6] for the ground-state transition, which were obtained at a deuteron energy of 52 MeV. The curve in Fig. 9 represents our DWBA results. The normalization between those data and the calculation was made at the most forward angular-distribution point. The estimated cross-section scale for the present ^{14}C data was then established by fitting our data for the ground-state transition to the DWBA calculation performed at the present bombarding energy (34.2-MeV equivalent deuteron energy). At the lower energy the ground-state data do not

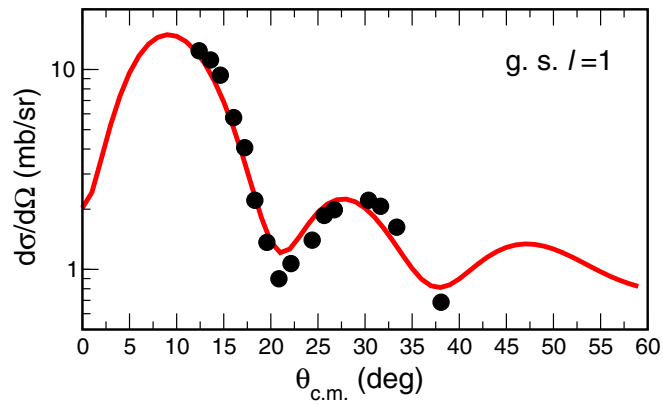

FIG. 9. Angular-distribution data for the ^{14}C$(d,{}^3\mathrm{He})^{13}$B$(3/2^-)$ ground-state transition from Ref. [6]. The curve represents a DWBA calculation described in the text.

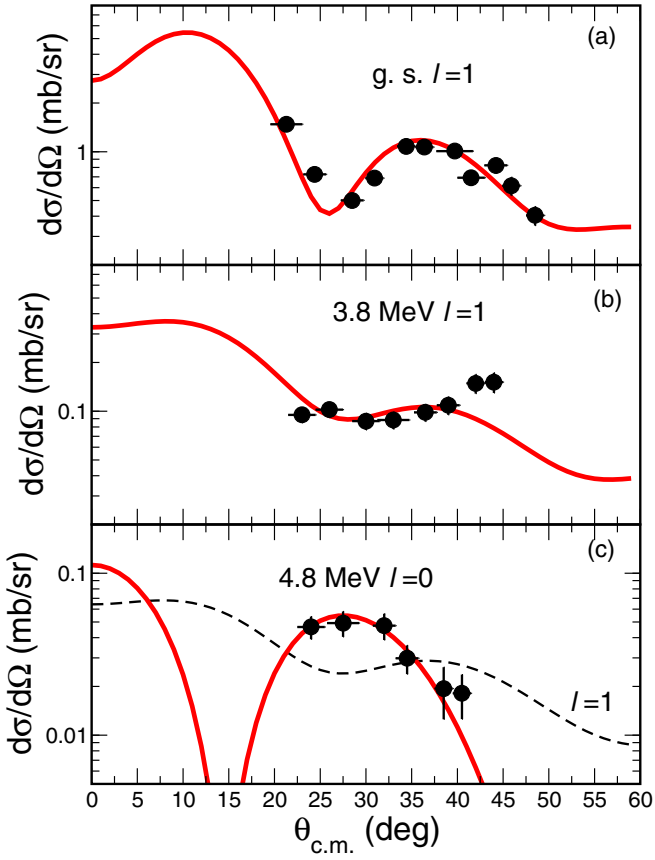

FIG. 10. Angular distributions for the (a) 0.0-, (b) 3.8-, and (c) 4.8-MeV transitions in ^{14}C(d,^{3}He)^{13}B. The curves represent DWBA calculations discussed in the text. For (a) and (b) the transitions are $\ell = 1$; for (c) the solid curve corresponds to $\ell = 0$. The dashed curve in (c) represents an $\ell = 1$ transition for comparison. When not visible, the vertical error bars are smaller than the plotting symbols. The horizontal error bars show the angular range for each point.

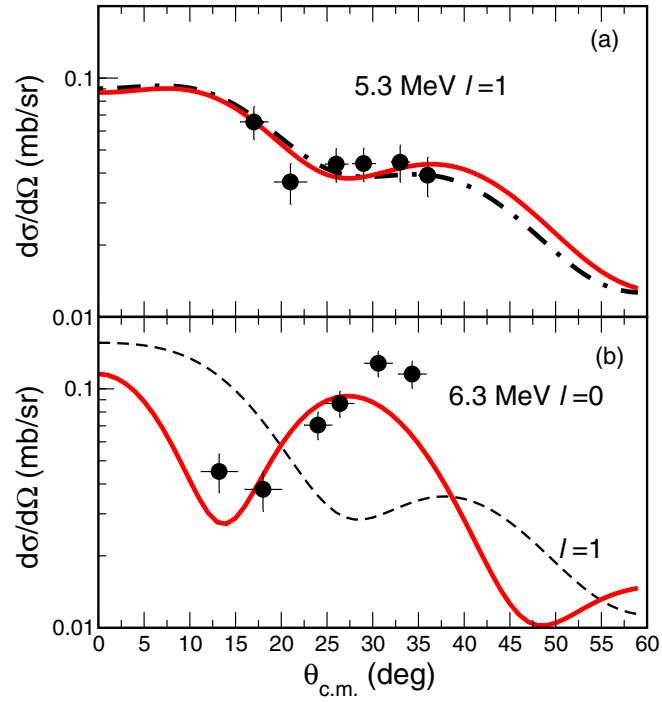

FIG. 11. Angular distributions for the (a) 5.3- and (b) 6.3-MeV transitions in ^{14}C(d,^{3}He)^{13}B. The curves represent DWBA calculations discussed in the text. The horizontal error bars show the angular range for each point. In (a) the solid and dot-dashed curves correspond to $\ell = 1$ with $J^\pi = 1/2^-$ or $3/2^-$. In (b), the solid and dashed curves represent $\ell = 0$ and 1 transitions, respectively. The DWBA curves in (b) are for illustration only.

reach the most forward angular-distribution maximum and we fit them to the curve over the entire angular range using a least-squares minimization procedure. This comparison established the cross-section scale for all other transitions in the ^{14}C(d,^{3}He)^{13}B reaction.

The resulting angular distributions for the present measurement appear in Figs. 10 and 11 for transitions to the particle-bound, and unbound states, respectively. For states above the neutron-separation threshold, the final states were treated as bound in the calculations. The error bars in all present data are statistical only and do not reflect any systematic uncertainty from the extrapolation done with the DWBA calculations. We estimate the additional systematic error in the overall cross-section scale of 30%. The following discussion and analyses do not depend on that scale.

Angular-distribution data for the ^{15}C(d,^{3}He)^{14}B reaction appear in Fig. 12. For the ^{15}C-beam data, the absolute beam intensity from the 0° monitor detector was more reliable, although still uncertain at the 30%–50% level. The 2^-_1 and 1^-_1 states were not fully resolved in this measurement, and the angular distribution for their combined yields appears in Fig. 12(a). Figure 12(b) shows the angular distribution for the broad presumed state at 1.8 MeV. The uncertainties shown are statistical and do not reflect the overall uncertainty in the absolute cross-section scale.

B. Distorted-wave Born Approximation calculations and spectroscopic factors

The deduced spectroscopic factors are defined as $C^2S \equiv \sigma_{\rm exp}/\sigma_{\rm DW}$, where C is the usual isospin Clebsch-Gordan coefficient, and $\sigma_{\rm exp}$ and $\sigma_{\rm DW}$ are the experimental and calculated DWBA cross sections, respectively. To reduce the sensitivity of the results to the overall uncertainty in the cross-section scale, we normalize the deduced spectroscopic factors such that the sum over all transitions equals 4. In the shell-model calculations discussed later, transitions to states below 7-MeV excitation energy exhaust more than 95% of this strength. The experimental values are given in Table II. There are additional uncertainties in the determination of spectroscopic factors. In the present experiment, the bombarding energies, which were the highest possible available from the accelerator at the time, are such that because of the very negative Q values the reactions are not well momentum-matched. This mismatch makes the interpretation of the calculations less reliable, especially for the excited states. It is also known that for very weak transitions with small spectroscopic factors, multistep processes not included in a direct-reaction treatment can be important.

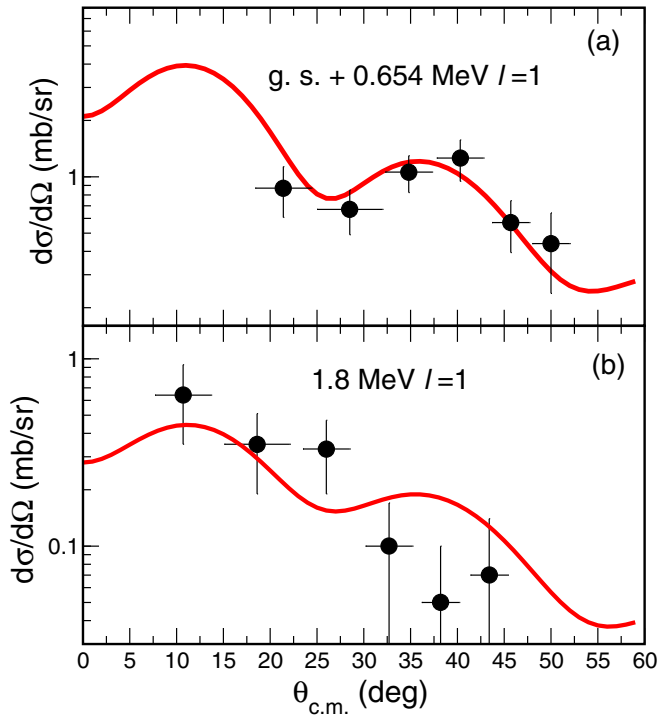

FIG. 12. Angular distribution for the (a) 2^-_1-1^-_1 doublet and (b) 1.8-MeV state in ^{14}B. The horizontal error bars show the angular range for each point. The DWBA curves represent $\ell = 1$ transitions as described in the text.

Schiffer *et al.* have shown that for such transitions there exist large variations in the values extracted from DWBA analyses when different reactions are considered [9]. The present data also do not include the forward-angle maxima of the angular distributions, adding more uncertainty to the normalization between the measured and calculated angular distributions, which is customarily performed at the first angular-distribution maximum. As described above, all spectroscopic factors are obtained from chi-square fits that include all of the measured points.

TABLE II. Spectroscopic factors $C^2S \equiv \sigma_{\rm exp}/\sigma_{\rm DWBA}$ for the ^{14,15}C$(d,^3$He$)^{13,14}$B reactions. The values are normalized such that the sum of C^2S over all transitions for each nucleus is 4.0.

	^{13}B		
E_X (MeV)	J^π	ℓ	C^2S
0.0	$3/2^-$	1	2.8 ± 0.30
3.8	$1/2^-$	1	0.7 ± 0.08
4.8	$(1/2^+)$	0	0.13 ± 0.02
5.3	$(1/2,3/2)^-$	1	0.35 ± 0.06
6.3	–	–	–
	^{14}B		
0.0	2^-	1	1.8 ± 0.35
0.654[a]	1^-	1	1.4 ± 0.30
1.8	2^-	1	0.8 ± 0.15

[a]Energy from Ref. [24].

1. $^{14}C \rightarrow {}^{13}B$

We have already discussed the ground state, where the angular distribution is well described by the $\ell = 1$ result. The angular distributions for the 3.8- and 5.3-MeV transitions are also consistent with $\ell = 1$. For the peak at $E_X = 3.8$ MeV, assuming that this peak comes only from the $1/2^-$ 3.71-MeV state, the deduced spectroscopic factor is 0.7 ± 0.08. The spectroscopic factor for the $\ell = 1$ transition at 5.3-MeV excitation energy is between 0.3 and 0.4, depending on whether the spin is assumed to be 1/2 or 3/2. The angular-distribution fits do not strongly distinguish between these two possibilities. For these negative-parity transitions, the deduced values of C^2S are between 10% and 25% of that of the ground state, larger than the 5% reported in Ref. [6]. Possible sources of this discrepancy are the momentum mismatch for these transitions and multistep processes as discussed above.

Data for the weak 4.8-MeV transition appear in Fig. 10(c). The angular distribution is inconsistent with $\ell = 1$; in this angle range it is much better described assuming an $\ell = 0$ transition, supporting a $J^\pi = 1/2^+$ spin-parity assignment. Assuming $J^\pi = 1/2^+$, the deduced spectroscopic factor is $C^2S = 0.13 \pm 0.02$, or about 5% of that of the ground state. A $J^\pi = 1/2^+$ assignment agrees with the results of Ota *et al.*, where the 4.83-MeV state was populated with a proton-stripping spectroscopic strength of $C^2S = 0.2 \pm 0.02$ [15]. These observations imply that $\pi(1s)^2(0p)^{-2}$ admixtures are present in the ^{14}C ground-state wave function. Ota *et al.* report that such a state is not well accommodated by spherical-basis shell-model calculations, and they interpreted this state as having a $\pi(1s_{1/2}) \otimes^{12}$ Be structure. Finally, the angular distribution for the narrow peak at $E_X \approx 6.3$ MeV appears in Fig. 11(b). The data are also inconsistent with $\ell = 1$ and more suggestive of an $\ell = 0$ transition. From the peak shape and background in Fig. 6(b), it is likely that this transition contains more than one unresolved state, likely with positive parity. Assuming this to be a single $1/2^+$ state, the corresponding spectroscopic factor would be approximately 20% of the ground-state value which is surprisingly large. Because of the uncertainties in the data and reaction-model analysis, however, we do not quote a C^2S value for this peak, and do not include it in the rescaling for the ^{13}B spectroscopic-factor sum in Table II.

Despite the quantitative uncertainties, the results listed in Table II make it clear that the proton-pickup strength from ^{14}C is distributed over several states in ^{13}B and probably more fragmented than was reported in Ref. [6]. We consider these observations in comparison to the predictions of shell-model calculations below.

2. $^{15}C \rightarrow {}^{14}B$

For the ^{15}C$(d,^3$He$)^{14}$B reaction, limited statistics make the experimental situation more challenging. We assume that the proton is removed only from a filled $0p_{3/2}$ orbital and, as before, the deduced spectroscopic factors are normalized to a total value of 4. This approach is likely not correct given the strength at higher excitation energies seen in the ^{13}B case, however, the data are not sufficient to identify very weak transitions. For the $2^-_1/1^-_1$ combination, the curve shown in Fig. 12(a) represents the sum of calculated angular

distributions for the two states. The angular distribution for the $2^-_1/1^-_1$ doublet is well described by an $\ell = 1$ transition as expected. Although the statistics for the presumed 2^-_2 resonance are poorer, this angular distribution is also reasonably well described by $\ell = 1$ proton removal. The individual spectroscopic strengths for the 2^-_1 and 1^-_1 states were obtained by decomposing the contributions to the two states using the $\ell = 0$ neutron-stripping spectroscopic factors from the ^{13}B$(d,p)^{14}$B measurement [16], with an additional $2J+1$ statistical weighting. The C^2S values for the three states are given in Table I.

V. SHELL-MODEL CALCULATIONS AND DISCUSSION

We have performed shell-model calculations for ^{14,15}C and ^{13,14}B with the WBT and WBP interactions [29] using the code NUSHELLX [30]. Here, the $0s_{1/2}$ orbital is inert and particles can occupy the $0p$ and $1s0d$ shells. The calculated ^{13,14}B excitation energies and spectroscopic overlaps for $^{14,15}\text{C} \rightarrow {}^{13,14}\text{B}$ are given in Table III, in the form of spectroscopic factors C^2S for $(d,{}^3\text{He})$. More detailed information about the wave functions for the nuclei of interest appears in Table IV, which shows the calculated neutron and proton occupation numbers for $0p$ and sd shells from the calculation with the WBP interaction. The occupation numbers from the WBT interaction are quite similar.

TABLE III. Shell-model excitation energies and spectroscopic factors for $(d,{}^3\text{He})$ for ^{13,14}B.

^{13}B	WBP		WBT	
J^π	E_X(MeV)	C^2S	E_X(MeV)	C^2S
$3/2^-$	0	3.51	0	3.50
$1/2^-$	3.868	0.19	3.848	0.19
$1/2^+$	4.305	0.003	4.665	0.003
$3/2^+$	4.934	0.008	5.033	0.009
$5/2^+$	5.263	0.029	5.387	0.029
$5/2^-$	5.481	0	5.396	0
$3/2^-$	5.598	0.003	5.66	0.004
$5/2^+$	6.436	0.003	6.608	0.005
$3/2^+$	6.689	0.019	6.696	0.018
$3/2^-$	6.797	0.056	6.711	0.051
$1/2^-$	6.829	0.001	6.857	0.001
$5/2^-$	6.915	0	7.048	0
^{14}B	WBP		WBT	
J^π	E_X(MeV)	C^2S	E_X(MeV)	C^2S
2^-	0	1.602	0	1.616
1^-	0.761	1.163[a]	0.72	1.159[a]
3^-	1.22	0	1.851	0
4^-	1.373	0	1.858	0
2^-	1.738	0.576	1.881	0.551
1^+	1.998	0.002	2.63	0.002
2^+	2.911	0.007[b]	3.021	.005[b]
2^+	3.848	<.001[b]	3.072	<0.001[b]
0^-	3.866	0	3.198	0
1^-	3.92	0.1359[a]	3.421	0.1759[a]

[a]Sum of $0p_{3/2}$ and $0p_{1/2}$.
[b]Sum of $0d_{3/2}$ and $0d_{5/2}$.

A. $^{14}\text{C} \rightarrow {}^{13}\text{B}$

As expected, the ground-state to ground-state transition is strongest with a calculated value of $C^2S = 3.5$. The next strongest transition is to the $1/2^-$ state with a spectroscopic factor of 0.19. Both values are in reasonable agreement with the experimental values from Ref. [6] although the ground- and first-excited state results from the present experiment are in only fair agreement with the calculations. The calculated spectroscopic factors for all other states are smaller, with no transition to any state below 7-MeV excitation energy having a value of C^2S greater than 0.06. The next strongest negative-parity state with a calculated value of $C^2S = 0.056$ is the second-excited $3/2^-$ level at 6.797 MeV. This calculated transition strength is of the same order-of-magnitude for the $1/2^-$ first-excited state, and could be associated with the $\ell = 1$ state observed in the data at 5.3 MeV. In all cases, the ratio of the calculated C^2S to that of the ground state is 5% or less.

As seen from Tables III and IV, the calculated low-lying positive-parity states have significant sd-shell neutron occupation with small overlaps with the ^{14}C ground state and small $(d,{}^3\text{He})$ spectroscopic factors. The largest is for the $5/2^+$ (≈ 5.3 MeV) state which has $C^2S = 0.029$. It is possible that if the experimental 3.68-MeV state corresponds to the lowest calculated $5/2^+$ excitation, it would be unresolved in the present experiment from the $1/2^-$ and could make a small contribution to the yield assigned to the $1/2^-$ transition. The next calculated positive-parity state with any appreciable spectroscopic factor is the second $3/2^+$ state near 6.7 MeV with $C^2S = 0.019$. This state would be populated through an $\ell = 2$ transition, however, the angular distribution for the 6.3-MeV peak more closely resembles $\ell = 0$ than $\ell = 2$. No $1/2^+$ state with any appreciable spectroscopic factor for $(d,{}^3\text{He})$ appears in the calculated spectrum below 13 MeV. Thus, low-lying $1/2^+$ states that can appear in $(d,{}^3\text{He})$ are difficult to accommodate within this shell-model analysis. A similar conclusion was also reached by Ota *et al.* in their analysis of the (α,t) reaction. Results for neutron stripping to ^{13}B were not well reproduced by shell-model calculations using these interactions [13].

In the work of Ref. [15] it was suggested that a $\pi(1s_{1/2}) \otimes {}^{12}$Be configuration may be responsible for the $1/2^+$ 4.83-MeV excitation. In our calculations, two $1/2^+$ states appear near 7.4 and 8.4 MeV; neither of these carries significant $\pi(sd)$ strength and instead each contains approximately 0.6–0.7 $0p_{1/2}$ protons and a mixture of $1s_{1/2}$ and $0d_{5/2}$ neutrons. Such configurations are less like proton "intruder" states but could instead be associated with configurations identified by Kanada-En'yo *et al.* which contained a $1\hbar\omega$ proton and a $2\hbar\omega$ neutron yielding a very deformed nucleus [31,32]. Ota *et al.* have argued that the energy of a high-lying $1/2^+$ state could be reduced by as much as 7 MeV from the deformation of the ^{12}Be core, and suggest a $\pi[220\frac{1}{2}]$ configuration as an alternate explanation of the $1/2^+$ 4.83-MeV state. Such a configuration led to a larger value of the proton-stripping spectroscopic factor in (α,t) and might also account for the observation of such an excitation in the present data. For that suggestion to be true, however, it requires more sd-proton strength in the ^{14}C ground-state wave function than appears in the present calculations.

TABLE IV. Shell-model occupation numbers for ^{14,15}C and ^{13,14}B with the WBP interaction.

			Protons					Neutrons				
Nucleus	E_X(MeV)	J^π	$0p_{3/2}$	$0p_{1/2}$	$0d_{5/2}$	$0d_{3/2}$	$1s_{1/2}$	$0p_{3/2}$	$0p_{1/2}$	$0d_{5/2}$	$0d_{3/2}$	$1s_{1/2}$
^{14}C	0.000	0^+	3.64	0.2	0.09	0.06	0.01	3.9	1.86	0.167	0.06	0.02
^{15}C	0.000	$1/2^-$	3.63	0.21	0.09	0.06	0.01	3.91	1.87	0.18	0.07	0.98
^{13}B	0.000	$3/2^-$	2.75	0.12	0.07	0.05	0.01	3.90	1.85	0.16	0.06	0.02
	3.848	$1/2^-$	1.91	0.90	0.10	0.07	0.02	3.84	1.78	0.25	0.09	0.05
	4.665	$1/2^+$	2.56	0.29	0.08	0.05	0.03	3.55	1.31	0.29	0.10	0.75
	5.033	$3/2^+$	2.50	0.35	0.07	0.05	0.02	3.66	1.21	0.58	0.13	0.42
	5.387	$5/2^+$	2.63	0.22	0.10	0.05	0.01	3.66	1.23	0.62	0.12	0.36
	5.396	$5/2^-$	1.91	0.90	0.11	0.06	0.02	3.82	1.74	0.29	0.10	0.05
	5.660	$3/2^-$	2.47	0.45	0.05	0.02	0.01	3.29	0.73	0.97	0.16	0.86
	6.608	$5/2^+$	2.59	0.27	0.09	0.05	0.01	3.58	1.30	0.52	0.13	0.47
	6.696	$3/2^+$	2.58	0.27	0.08	0.05	0.02	3.68	1.22	0.43	0.10	0.57
	6.711	$3/2^-$	1.59	1.21	0.11	0.07	0.02	3.71	1.60	0.44	0.11	0.13
	6.857	$1/2^-$	2.14	0.75	0.06	0.04	0.01	3.09	0.95	0.97	0.16	0.84
^{14}B	0.000	2^-	2.73	0.15	0.07	0.05	0.01	3.92	1.87	0.43	0.07	0.71
	0.761	1^-	2.72	0.14	0.07	0.05	0.01	3.92	1.86	0.28	0.08	0.86
	1.220	3^-	2.72	0.16	0.07	0.05	0.01	3.92	1.88	1.11	0.07	0.03
	1.373	4^-	2.70	0.18	0.06	0.04	0.01	3.92	1.88	1.13	0.06	0.02
	1.738	2^-	2.70	0.18	0.06	0.04	0.01	3.91	1.87	0.85	0.08	0.29
	1.998	1^+	2.56	0.33	0.05	0.04	0.02	3.79	1.14	0.95	0.15	0.97
	2.911	2^+	2.57	0.32	0.06	0.04	0.01	3.81	1.12	1.05	0.16	0.86
	3.848	2^+	2.54	0.36	0.06	0.03	0.01	3.77	1.16	1.23	0.17	0.66
	3.866	0^-	2.05	0.78	0.11	0.05	0.01	3.77	1.47	0.91	0.13	0.73
	3.920	1^-	2.51	0.33	0.08	0.06	0.02	3.88	1.82	1.01	0.11	0.19

B. ^{15}C → ^{14}B

For ^{15}C → ^{14}B, the only low-lying excitations with any strength in $(d,^3\mathrm{He})$ are the pairs of 2^- and 1^- states formed by the coupling of sd-shell neutrons with a $0p_{3/2}$ proton hole. The $0d_{5/2}$ neutron can also make states with any strength in $(d,^3\mathrm{He})$ are the pairs of 2^- and 1^- states formed by the coupling of sd-shell neutrons with a $0p_{3/2}$ proton hole. The $0d_{5/2}$ neutron can also make states with $J^\pi = (3,4)^-$ and such levels have been observed in ^{14}B; these are not populated in $(d,^3\mathrm{He})$. The excited 1_2^- state appears above 3-MeV excitation energy in each calculation, suggesting that an experimental counterpart would be broad and very difficult to observe, especially with the small calculated C^2S value of 0.136 or 0.176, depending on the interaction. We can compare the calculated ratios of the proton-removal spectroscopic factors to the observed values in Table II. The calculated ratio of $C^2S(1_1^-)/C^2S(2_1^-)$ from either interaction is 0.72, in good agreement with the experimental value of 0.8 ± 0.12. For the excited 2_2^- state, the calculated ratio $C^2S(2_2^-)/C^2S(2_1^-)$ is 0.36, approximately consistent with the experimental value of 0.44 ± 0.07.

VI. CONCLUSIONS

The results of the present measurements of the $(d,^3\mathrm{He})$ reaction provide new information about ground-state proton wave functions in ^{14}C, as well as for the properties of excited states in both ^{13,14}B. For ^{14}C → ^{13}B, weak transitions are observed to states that likely possess $0p_{1/2}$ proton character in addition to the $1/2^-$ state at 3.71 MeV. A very weak $\ell = 0$ transition may be associated with a possible $1/2^+$ state in ^{13}B that was suggested as a proton-intruder level from the ^{12}Be$(\alpha,t)^{13}$B reaction. Such an excitation is not well described by shell-model calculations and its observation could support the picture of a deformed state at low excitation energy in ^{13}B given by Ota *et al.* The present measurements suggest that more excitations beyond the ground state in ^{13}B are populated in this reaction than were previously suspected.

For ^{14}B, the data confirm the broad excited 2^- state reported in prior measurements. The relative proton-pickup spectroscopic factors are consistent with shell-model calculations, as well as expectations based on prior measurements of neutron transfer with the ^{13}B$(d,p)^{14}$B reaction. As the present experiment was performed at a bombarding energy where the reactions are not well matched in momentum for all excitations, further studies at higher bombarding energies with more intense beams could prove fruitful, as could similar studies of proton removal from even more neutron-rich carbon isotopes. Such measurements await the development of future radioactive-beam facilities.

ACKNOWLEDGMENTS

The authors would like to acknowledge the hard work of the support and operations staff of the ATLAS facility, and thank B. A. Brown for his assistance with the shell-model calculations. This material is based upon work supported by the U.S. Department of Energy, Office of Science, Office of Nuclear Physics, under Grants No. DE-FG02-04ER41320, No. DE-SC0014552, and No. DE-AC02-06CH11357, and the U.S.

National Science Foundation under Grant No. PHY-1068217. This research used resources of the Argonne National Laboratory ATLAS Accelerator Facility, which is a DOE Office of Science User Facility.

[1] D. R. Inglis, Phys. Rev. **87**, 915 (1952).
[2] P. G. Roos, S. M. Smith, V. K. C. Cheng, G. Tibell, A. A. Cowley, and R. A. J. Riddle, Nucl. Phys. A **255**, 187 (1975).
[3] O. Karban, A. K. Basak, J. B. A. England, G. C. Morrison, J. M. Nelson, S. Roman, and G. G. Shute, Nucl. Phys. A **269**, 312 (1976).
[4] J. D. Cossairt, S. B. Talley, D. P. May, R. E. Tribble, and R. L. Spross, Phys. Rev. C **18**, 23 (1978).
[5] J. Van de Wiele, H. Langevin-Joliot, F. Jourdan, J. Guillot, E. Gerlic, L. H. Rosier, A. Willis, C. Djalali, M. Morlet, E. Tomasi-Gustafsson, N. Blasi, S. Micheletti, and S. Y. van der Werf, Phys. Rev. C **50**, 2935 (1994).
[6] G. Mairle and G. J. Wagner, Nucl. Phys. A **253**, 253 (1975).
[7] F. Flavigny, A. Gillibert, L. Nalpas, A. Obertelli, N. Keeley, C. Barbieri, D. Beaumel, S. Boissinot, G. Burgunder, A. Cipollone, A. Corsi, J. Gibelin, S. Giron, J. Guillot, F. Hammache, V. Lapoux, A. Matta, E. C. Pollacco, R. Raabe, M. Rejmund, N. de Séreville, A. Shrivastava, A. Signoracci, and Y. Utsuno, Phys. Rev. Lett. **110**, 122503 (2013).
[8] J. P. Schiffer, C. R. Hoffman, B. P. Kay, J. A. Clark, C. M. Deibel, S. J. Freeman, A. M. Howard, A. J. Mitchell, P. D. Parker, D. K. Sharp, and J. S. Thomas, Phys. Rev. Lett. **108**, 022501 (2012).
[9] J. P. Schiffer, C. R. Hoffman, B. P. Kay, J. A. Clark, C. M. Deibel, S. J. Freeman, M. Honma, A. M. Howard, A. J. Mitchell, T. Otsuka, P. D. Parker, D. K. Sharp, and J. S. Thomas, Phys. Rev. C **87**, 034306 (2013).
[10] S. Cohen and D. Kurath, Nucl. Phys. A **101**, 1 (1967).
[11] I. Talmi and I. Unna, Phys. Rev. Lett. **4**, 469 (1960).
[12] C. R. Hoffman, B. P. Kay, and J. P. Schiffer, Phys. Rev. C **89**, 061305(R) (2014).
[13] B. B. Back, S. I. Baker, B. A. Brown, C. M. Deibel, S. J. Freeman, B. J. DiGiovine, C. R. Hoffman, B. P. Kay, H. Y. Lee, J. C. Lighthall, S. T. Marley, R. C. Pardo, K. E. Rehm, J. P. Schiffer, D. V. Shetty, A. W. Vann, J. Winkelbauer, and A. H. Wuosmaa, Phys. Rev. Lett. **104**, 132501 (2010).
[14] H. Iwasaki, A. Dewald, C. Fransen, A. Gelberg, M. Hackstein, J. Jolie, P. Petkov, T. Pissulla, W. Rother, and K. O. Zell, Phys. Rev. Lett. **102**, 202502 (2009).
[15] S. Ota, S. Shimoura, H. Iwasaki, M. Kurokawa, S. Michimasa, N. Aoi, H. Baba, K. Demichi, Z. Elekes, T. Fukuchi, T. Gomi, S. Kanno, S. Kubono, K. Kurita, H. Hasegawa, E. Ideguchi, N. Iwasa, Y. U. Matsuyama, K. L. Yurkewicz, T. Minemura, T. Motobayashi, T. Murakami, M. Notani, A. Odahara, A. Saito, H. Sakurai, E. Takeshita, S. Takeuchi, M. Tamaki, T. Teranishi, Y. Yanagisawa, K. Yamada, and M. Ishihara, Phys. Lett. B **666**, 311 (2008).
[16] S. Bedoor, A. H. Wuosmaa, J. C. Lighthall, M. Alcorta, B. B. Back, P. F. Bertone, B. A. Brown, C. M. Deibel, C. R. Hoffman, S. T. Marley, R. C. Pardo, K. E. Rehm, A. M. Rogers, J. P. Schiffer, and D. V. Shetty, Phys. Rev. C **88**, 011304(R) (2013).
[17] G. C. Ball, G. J. Costa, W. G. Davies, J. S. Forster, J. C. Hardy, and A. B. McDonald, Phys. Rev. Lett. **31**, 395 (1973).
[18] A. H. Wuosmaaa, J. P. Schiffer, B. B. Back, C. J. Lister, and K. E. Rehm, Nucl. Instrum. Methods Phys. Res., Sect. A **580**, 1290 (2007).
[19] J. C. Lighthall, B. B. Back, S. I. Baker, S. J. Freeman, H. Y. Lee, B. P. Kay, S. T. Marley, K. E. Rehm, J. E. Rohrer, J. P. Schiffer, D. V. Shetty, A. W. Vann, J. R. Winkelbauer, and A. H. Wuosmaa, Nucl. Instrum. Methods Phys. Res., Sect. A **622**, 97 (2010).
[20] B. Harss, R. C. Pardo, K. E. Rehm, F. Borasi, J. P. Greene, R. V. F. Janssens, C. L. Jiang, J. Nolen, M. Paul, J. P. Schiffer, R. E. Segel, J. Specht, T. F. Wang, P. Wilt, and B. Zabransky, Rev. Sci. Instrum. **71**, 380 (2000).
[21] K. E. Rehm, J. P. Greene, B. Harss, D. Henderson, C. L. Jiang, R. C. Pardo, B. Zabransky, and M. Paul, Nucl. Instrum. Methods Phys. Res., Sect. A **647**, 3 (2011).
[22] A. H. Wuosmaa, J. P. Schiffer, S. Bedoor, M. Albers, M. Alcorta, S. Almaraz-Calderon, B. B. Back, P. F. Bertone, C. M. Deibel, C. R. Hoffman, J. C. Lighthall, S. T. Marley, R. C. Pardo, K. E. Rehm, and D. V. Shetty, Phys. Rev. C **90**, 061301 (2014).
[23] F. Azjenberg-Selove, Nucl. Phys. A **523**, 1 (1991).
[24] R. Kanungo, Z. Elekes, H. Baba, Zs. Dombradi, Zs. Fulop, J. Gibelin, A. Horvath, Y. Ichikawa, E. Ideguchi, N. Iwasa, H. Iwasaki, S. Kawai, Y. Kondo, T. Motobayashi, M. Notani, T. Ohnishi, A. Ozawa, H. Sakurai, S. Shimoura, E. Takeshita, S. Takeuchi, I. Tanihata, Y. Togano, C. Wu, Y. Yamaguchi, Y. Yanagisawa, A. Yoshida, and K. Yoshida, Phys. Lett. B **608**, 206 (2005).
[25] M. H. Mcfarlane and S. C. Pieper, Argonne National Laboratory Report No. ANL-76-11, Rev. 1 (Argonne National Laboratory, Argonne, 1978).
[26] Haixia An and Chonghai Cai, Phys. Rev. C **73**, 054605 (2006).
[27] D. Y. Pang, P. Roussel-Chomaz, H. Savajols, R. L. Varner, and R. Wolski, Phys. Rev. C **79**, 024615 (2009).
[28] I. Brida, S. C. Pieper, and R. B. Wiringa, Phys. Rev. C **84**, 024319 (2011).
[29] E. K. Warburton and B. A. Brown, Phys. Rev. C **46**, 923 (1992).
[30] B. A. Brown and W. D. M. Rae, Nucl. Data Sheets **120**, 115 (2014).
[31] Y. Kanada-En'yo, Y. Taniguchi, and M. Kimura, Nucl. Phys. A **805**, 392c (2008).
[32] Yoshiko Kanada-En'yo, Phys. Rev. C **91**, 014315 (2015).